Potential Predictability of Summer Mean Precipitation in a Dynamical Seasonal Prediction System with Systematic Error Correction

IN-SIK KANG AND JUNE-YI LEE

School of Earth and Environmental Sciences, Seoul National University, Seoul, South Korea

CHUNG-KYU PARK

Climate Prediction Division, Korea Meteorological Administration, Seoul, South Korea

(Manuscript received 5 November 2002, in final form 7 February 2003)

ABSTRACT

Potential predictability of summer mean precipitation over the globe is investigated using data obtained from seasonal prediction experiments for 21 yr from 1979 to 1999 using the Korea Meteorological Administration–Seoul National University (KMA–SNU) seasonal prediction system. This experiment is a part of the Climate Variability and Predictability Program (CLIVAR) Seasonal Model Intercomparison Project II (SMIP II). The observed SSTs are used for the external boundary condition of the model integration; thus, the present study assesses the upper limit of predictability of the seasonal prediction system. The analysis shows that the tropical precipitation is largely controlled by the given SST condition and is thus predictable, particularly in the ENSO region. But the extratropical precipitation is less predictable due to the large contribution of the internal atmospheric processes to the seasonal mean. The systematic error of the ensemble mean prediction is particularly large in the subtropical western Pacific, where the air–sea interaction is active and thus the two-tier approach of the present prediction experiment is not appropriate for correct predictions in the region.

The statistical postprocessing method based on singular value decomposition corrects a large part of the systematic errors over the globe. In particular, about two-thirds of the total errors in the western Pacific are corrected by the postprocessing method. As a result, the potential predictability of the summer-mean precipitation is greatly enhanced over most of the globe by the statistical correction method; the 21-yr-averaged pattern-correlation value between the predictions and their observed counterparts is changed from 0.31 before the correction to 0.48 after the correction for the global domain and from 0.04 before the correction to 0.26 after the correction for the Asian monsoon and the western Pacific region.

1. Introduction

Water resources in the Asian monsoon region depend largely on the precipitation during the summer rainy season (Ramage 1971; Terjung et al. 1989; Wang and LinHo 2002). Thus, the prediction of summer monsoon precipitation has been an important issue in Asian monsoon countries, and it has a long history, dating back to the 1870s (Normand 1953). In recent years, several investigators have attempted monsoon predictions using a state-of-art dynamical tool, namely, general circulation models (GCMs; Sperber and Palmer 1996; Goswami 1998; Sperber et al. 2001; Kang et al. 2002a,b). The GCM studies, however, show the limitations of dynamical monsoon prediction. It is known that the present skill of dynamical seasonal prediction is limited by several factors, mainly inherent nonlinear characteristics of the atmosphere and the inaccurate performance of current GCMs. In the present study, we investigate what portion of the predictability is affected by the atmospheric internal and external processes and develop a statistical tool for correcting the GCM predictions.

Regional climate anomalies can arise from many sources of external forcings, such as ocean and land anomalies, and internal processes inherent in the atmosphere. The internal processes of the atmosphere are mainly associated with atmospheric instability mechanisms with shorter time scales and involve stochastic nonlinear processes. Such internal processes are known to have a predictability of only a few days (Lorenz 1960). Thus, the seasonal predictability is very much limited by the atmospheric internal processes. On the other hand, the slowly varying external forcings, such as SST anomalies, produce the atmospheric responses that might result in a predictable signal of the seasonal anomalies. The ratio of external to internal components of the seasonal anomalies is an important parameter for the potential predictability. Recently potential predict-

Corresponding author address: Prof. In-Sik Kang, Climate Environment System Research Center, Seoul National University, Kanwak-Gu, Seoul 151-742, South Korea.
E-mail: kang@climate.snu.ac.kr

ability has been estimated using an ensemble of climate simulations, where all members are forced by the same observed SST but are started from slightly different atmospheric initial conditions (Dix and Hunt 1995; Kumar and Hoerling 1995; Stern and Miyakoda 1995; Zwiers 1996). The basic idea of this approach is that the sensitivity to the initial conditions can be used to quantify the random (internal) component of the seasonal anomalies, whereas the relative similarity between ensemble members can be considered as the atmospheric response to the external forcing. Thus, the ensemble mean can be considered to be the external component of the prediction forced by the SST forcing, and the deviation from the ensemble mean to be the stochastic internal component of the prediction.

In the present study, the potential predictability is measured by the ratio between the external and internal components of the seasonal prediction using a standard statistical tool for this kind of problem: analysis of variance (ANOVA), which is detailed in the regional study of Rowell et al. (1995) and the global study of Rowell (1998). The data utilized are from the Seasonal Model Intercomparison Project II (SMIP II) initiated by the Climate Variability and Predictability Program (CLIVAR)/Working Group of Seasonal to Interannual Prediction (WGSIP). The purpose of SMIP II is to evaluate the current dynamical seasonal prediction systems in a simplified framework, where the lower boundary conditions are prescribed with the observed SSTs for the 20-yr period of 1979–98. Therefore, the uncertainty of SST prediction is avoided in SMIP II, and this study provides the upper limit of the potential predictability.

The low skill of the dynamical seasonal prediction is due not only to the atmospheric internal processes but also to the model's inability to produce the atmospheric responses to external forcings, particularly the SST anomalies. This model bias in the external component appears in a systematic way in both the climatological mean and the anomaly component. The mean bias can be corrected by subtracting the prediction climatology from the seasonal prediction of each individual year. The systematic error of the anomaly component is related to the incorrect performance of the GCM in simulating the anomalies, predominantly forced by the SST anomalies. It is noted that a slight shift of the spatial pattern of variability in the model can result in a substantial drop in skill scores when the skill is measured based on the performance at individual grid points. A major part of this systematic error can be corrected by using a statistical relationship between the prediction and observed anomalies, the so-called coupled pattern technique (Graham et al. 1994). The most commonly used methodologies of the coupled pattern technique are based on singular value decomposition analysis (SVDA) and canonical correlation analysis (CCA). Ward and Navarra (1997) applied SVDA to simultaneous fields of GCM-simulated precipitation and observed precipitation to correct the errors in the model response to SST forcing. CCA has been widely used as a statistical seasonal prediction system (Barnett and Preisendorfer 1987; Barnston 1994). A recent study by Feddersen et al. (1999) demonstrated that the postprocessed results are not sensitive to the choice among the methods based on the CCA, SVD, and EOF decompositions. In the present study, the postprocessing procedure of the error correction is developed based on the SVD analysis, which is similar to the method used by Feddersen et al. (1999), and the potential predictability of the seasonal prediction is assessed after applying the correction procedure. By comparing the potential predictabilities with and without the correction, we can evaluate how the postprocessing of the error correction enhances the predictability in the regions of interest.

Section 2 describes the seasonal prediction system, seasonal prediction experiments, and the data utilized in the present study. In section 3, the summer-mean climatology of the predicted precipitation and the interannual variability of the summer mean are compared to the observed counterparts. The interannual variance of the predicted precipitation is decomposed to the external component forced by SST anomalies and the internal component of the model. Section 4 shows the model skill of the seasonal-mean precipitation without correction. Section 5 describes the postprocessing method for systematic error correction and the verification method of the seasonal prediction. The potential predictability of the seasonal prediction after correction is assessed by applying the postprocessing methods to the prediction data. A summary and concluding remarks are given in section 6.

2. Data

The data utilized in the present study are produced by the Korea Meteorological Administration–Seoul National University (KMA–SNU) seasonal prediction system as part of the Seasonal Prediction Model Intercomparison Project II (SMIP II). The SMIP II was initiated by the CLIVAR/WGSIP in 2000 as a follow-up program to the SMIP, which focused on one-season-lead prediction for four summers and four winters (Kusunoki et al. 2001). The SMIP II extends the prediction target to two seasons for all four seasons (winter, spring, summer, autumn) for the 21 yr from 1979 to 1999, requiring each participating center to carry out 10 ensemble integrations for 7 months with observed initial conditions of 0000 and 1200 UTC 24–28 February for spring and summer prediction, 0000 and 1200 UTC 27–31 May for summer and fall prediction, 0000 and 1200 UTC 27–31 August for autumn and winter prediction, and 0000 and 1200 UTC 26–30 November for winter and spring prediction. The observed SSTs are prescribed for the integration. Therefore, the SMIP II can estimate the upper bound of seasonal predictability but not the actual predictability. (See the details of SMIP II online at http://www-pcmdi.llnl.gov/smip.)

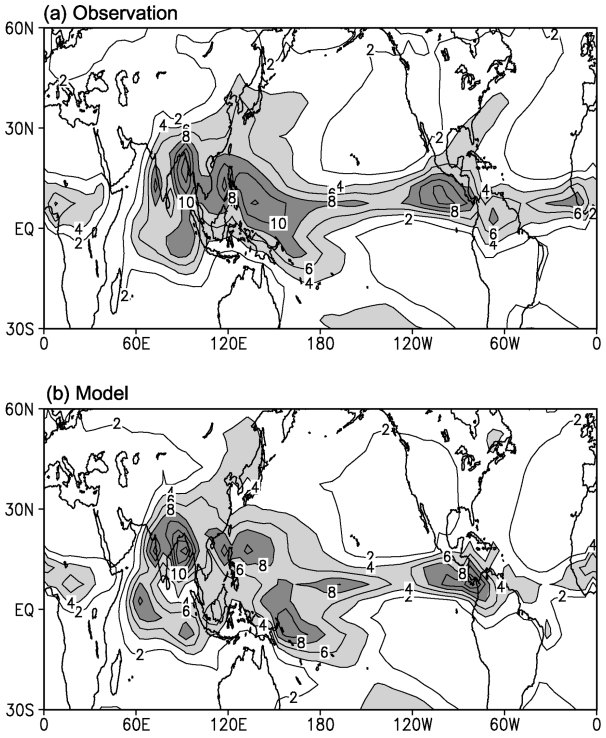

FIG. 1. Climatological summer-mean precipitation: (a) observation, (b) model. Contour interval is 2 mm day^{-1}.

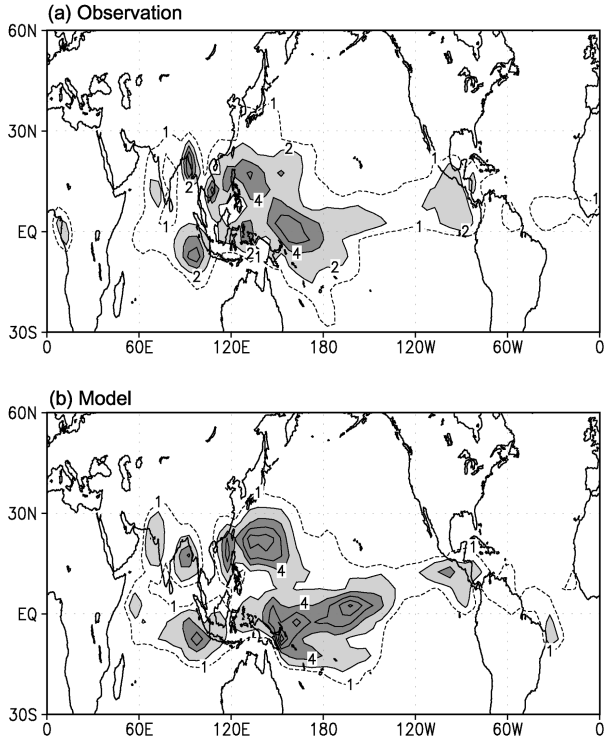

FIG. 2. Variance of the interannual variation of the summer-mean precipitation for the 21 yr from 1979 to 1999: (a) observation and (b) all members of the prediction (10 members $\times$ 21 yr). The contour interval is 2 mm^2 day^{-2} and the dashed line indicates 1 mm^2 day^{-2}.

The KMA–SNU model is a global spectral model with a spectral truncation at T63 and it has 21 vertical levels. The major physical parameterizations adapted in the model include the relaxed Arakawa–Shubert scheme for the convection (Moorthi and Suarez 1992), the *k*-distribution radiation scheme for the shortwave and longwave radiation (Nakajima and Tanaka 1986), the Bonan (1998) scheme for the land surface processes, a nonlocal planetary boundary layer scheme (Holtslag and Boville 1993), and an orographic gravity wave drag parameterization (McFarlane 1987). Kim et al. (1998) showed that the model is capable of simulating the climatology and interannual variations of global precipitation and circulation statistics reasonably well. The model performance in simulating the summer monsoon statistics and the 1997/98 El Niño anomalies compared to those of the other 10 current GCMs that participated in the CLIVAR/Monsoon GCM Intercomparison Project can be found in Kang et al. (2002a,b).

The present study focuses on the predictability of seasonal-mean rainfall for boreal summer. For brevity, hereafter ''boreal summer'' is abbreviated to ''summer.'' The prediction data utilized consist of 10 members of summer-mean precipitation for the 21 summers of 1979–99. The horizontal interval of the data converted is 2.5° in latitude and 2.5° in longitude. The observed precipitation data utilized are from the Climate Prediction Center (CPC) Merged Analysis of Precipitation (CMAP) dataset (Xie and Arkin 1997).

3. Climatological mean and interannual variability

The summer-mean climatology of predicted precipitation (Fig. 1b) is compared to the corresponding observed precipitation (Fig. 1a). Figure 1a is based on the observed summer means for the 21 yr, and Fig. 1b is obtained by averaging the 210 members of the prediction, 21 summers $\times$ 10 members. The observation shows that a large amount of precipitation appears in the Asian monsoon regions of southern and eastern Asia, the tropical western Pacific, and the intertropical convergence zone along the equatorial Pacific. The observed precipitation pattern is reasonably well simulated by the model, although some deficiencies are seen in the simulated field, particularly too much dryness in the equatorial western Indian Ocean and south of the Philippines, and the maximum precipitation region in the western Pacific is shifted to the north by about 5°–10°. Also note that the East Asian rainfall belt from eastern China toward the Korean peninsula is missing in the prediction field. A similar failure of the prediction appears off the east coast of North America.

The interannual variability of the summer-mean precipitation is examined in terms of its variance, the mean square of the anomalies. The anomaly here is defined as the deviation of the summer-mean precipitation from its climatology. Figure 2a shows the variance of the observed summer-mean precipitation for the 21 yr. The

spatial pattern of Fig. 2a is similar to that of Fig. 1a, indicating that large variability appears in the regions of large mean precipitation. Figure 2b is the corresponding variance of the prediction, based on all 210-member predictions for the 21 yr, which will be referred to as the total variance of the prediction. As in the observation, the spatial distribution of the simulated variance appears to be similar to that of the simulated mean. The simulated variance is larger than that of the observed in most of the Tropics. The difference between the observed and the simulated may be partly due to the difference in the number of samples. But, the larger variance of the prediction seems to be related to the larger summer mean of the prediction compared to the observed, particularly in the Pacific. The northward shift of the variance center in the prediction field in the northern western Pacific is also seen in the predicted summer mean.

The total variance (σ^2_{TOT}) is divided into the external (σ^2_{SST}) and internal variances [σ^2_{INR}; Rowell (1996)]. The internal variance is estimated by the 21-summer-mean variance of the deviations of the 10 members from the ensemble mean of each year, which can be expressed as

$$\sigma^2_{\mathrm{INR}} = \frac{1}{N(n-1)} \sum_{i=1}^{N} \sum_{j=1}^{n} (x_{ij} - \overline{x_i})^2, \qquad (1)$$

where x is the precipitation, i indicates the individual year, $N = 21$, j is the ensemble member, and $n = 10$. Here, $\overline{x_i}$ is the ensemble mean. The external variance is obtained by the mean square of the deviation of each year's ensemble mean from the climatological mean and considering the bias correction as used in Rowell (1996):

$$\sigma^2_{\mathrm{SST}} = \sigma^2_{\mathrm{EN}} - \frac{1}{n}\sigma^2_{\mathrm{INR}}, \quad \text{and}$$

$$\sigma^2_{\mathrm{EN}} = \frac{1}{N-1} \sum_{i=1}^{N} (\overline{x_i} - \overline{\overline{x}})^2, \qquad (2)$$

where $\overline{\overline{x}}$ is the climatological mean of the ensemble mean $\overline{\overline{x}} = [1/(Nn)] \sum_{i=1}^{N} \sum_{j=1}^{n} x_{ij}$. It is noted that the sum of the external and internal variances expressed above is equal to the total variance.

The spatial pattern of the external variance shown in Fig. 3a is similar to that of the total variance and contributes most of the total variance. The ratio of the external part to the internal part is shown in Fig. 3c. In most of the tropical regions, the external variance is much larger than the internal part. In the extratropics, on the other hand, the internal variance is bigger than the external variance. This may be due to the insensitivity of the atmosphere to the extratropical SST and the relatively large stochastic processes of the extratropical atmosphere associated with internal instability mechanisms. The figure indicates that the tropical rainfall is less controlled by the atmospheric internal processes and more predictable for a given SST condition than the extratropical rainfall. On the other hand, the extratropical rainfall variability is internal and therefore less predictable.

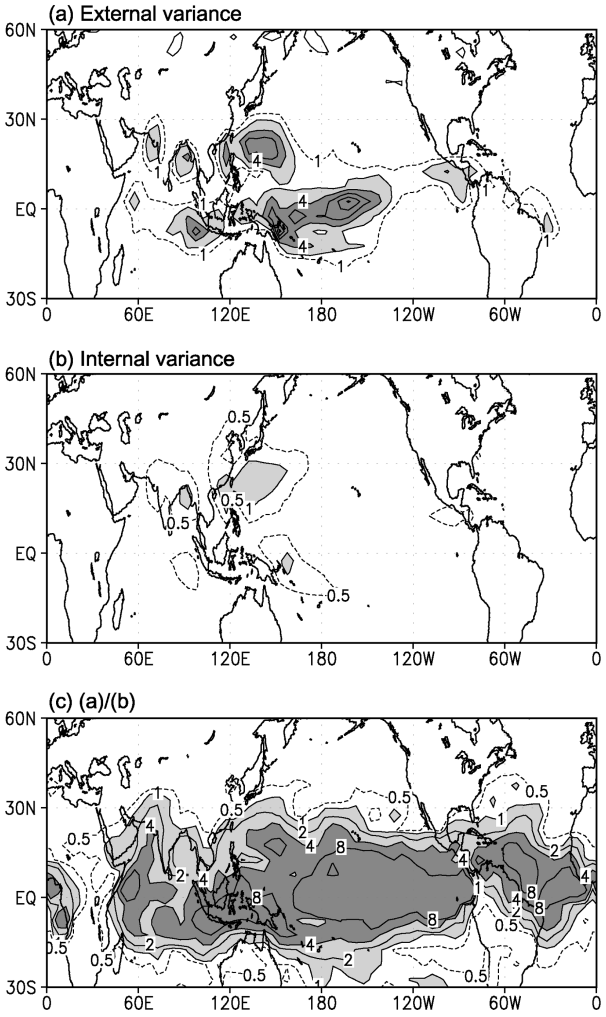

FIG. 3. (a) Forced variance of the precipitation based on the ensemble average of each year. The contour interval is 2 mm^2 day^{-2} and the dashed line indicates 1 mm^2 day^{-2}. (b) Internal variance based on the deviation of individual members from the ensemble average. The contour interval is 1 mm^2 day^{-2} and the dashed line indicates 0.5 mm^2 day^{-2}. (c) Ratio of (a) to (b). Contour levels are 1, 2, 4, 8, and 16 and the dashed line indicates 0.5.

As seen in Fig. 3c, the tropical rainfall variations are shown to be mainly controlled by the SST anomalies. Thus, the tropical rainfall has a large potential predictability, if the model simulates the responses to SST anomalies reasonably well. But, the model is incomplete and systematic errors due to model bias are expected in the ensemble mean prediction. Therefore, the ratio shown in Fig. 3c shows the upper limit of the predictability. The systematic error is estimated as the difference between the ensemble mean of the model prediction and the corresponding observation. The variance of the systematic error is shown in Fig. 4a. It is interesting to note that large errors appear in the regions of large response to the SST anomaly shown in Fig. 3a,

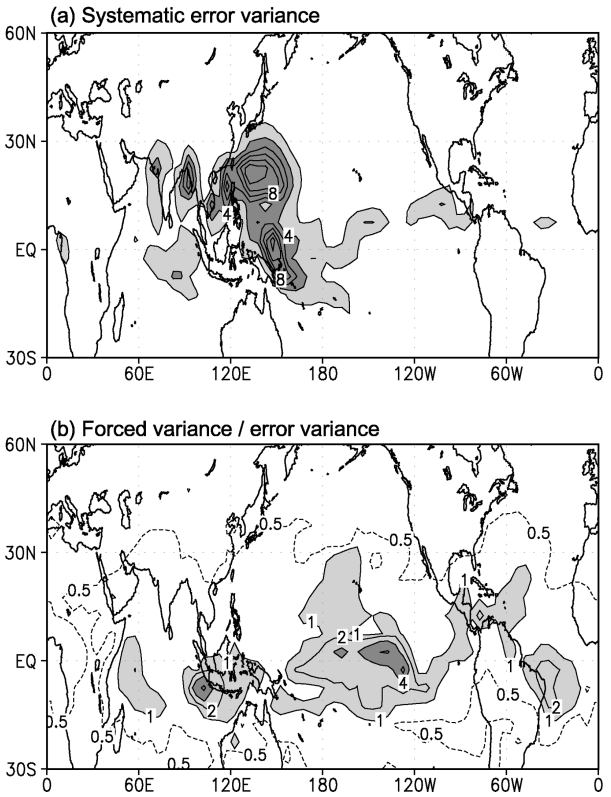

FIG. 4. (a) Variance of the systematic error, the difference between the ensemble average of the prediction and the corresponding observation. The contour interval is 2 mm^2 day^{-2}. (b) Ratio between the variances of the ensemble mean and the systematic error. Contour levels are 1, 2, 4, and 8 and the dashed line indicates 0.5.

particularly in the western Pacific. The ratio of the external variance to the error variance is shown in Fig. 4b. If the ratio is bigger than one, the prediction signal can be considered to be larger than the error. Such regions appear in the central equatorial Pacific, the tropical Indian Ocean, and near the northeastern coast of South America.

4. Correlation skill of the prediction without correction

The prediction skill of the model can be measured by the anomaly correlation between the predictions and the corresponding observations for the 21 yr. Figure 5a shows the spatial distribution of the correlation coefficient between the ensemble mean and the corresponding observation. As expected, the regions of large ratio shown in Fig. 4b coincide with the regions of large correlation. The figures indicate that the skill of the model prediction is relatively high only in parts of the Tropics, particularly in the central and eastern tropical Pacific, the Indonesian subcontinent, and east of Brazil. It is also noted that the correlation is negative in the tropical western Pacific and tropical central Indian Ocean, where the external response has a large systematic error (systematic error larger than the ensemble mean; Fig. 4c). Therefore, the relatively poor skill in the western Pacific and Indian Oceans is due to the model bias, probably due to poor parameterizations of the physical processes.

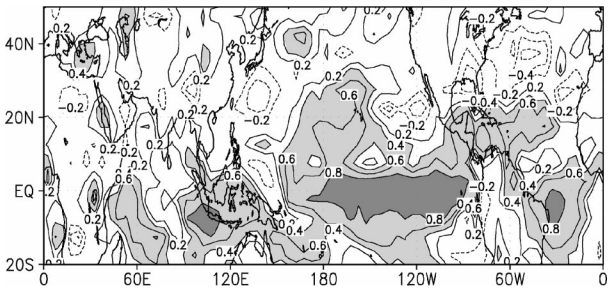

FIG. 5. Distribution of the correlation coefficient between the observed and the simulated ensemble-mean precipitation at each grid point. Contour interval is 0.2. Zero line is not drawn.

The spatial correlation over the globe between the ensemble mean of predicted summer-mean precipitation anomalies at each year and the corresponding observed precipitation anomaly is shown in Fig. 6a with shaded bars. The spatial correlation for the ENSO–monsoon region (30°S–30°N and 40°E–80°W) is also shown in Fig. 6a with open bars. The spatial correlation of each ensemble member is shown with crosses. The global correlation varies from 0.08 in 1981 to 0.50 in 1987. The correlation of the ENSO–monsoon region varies

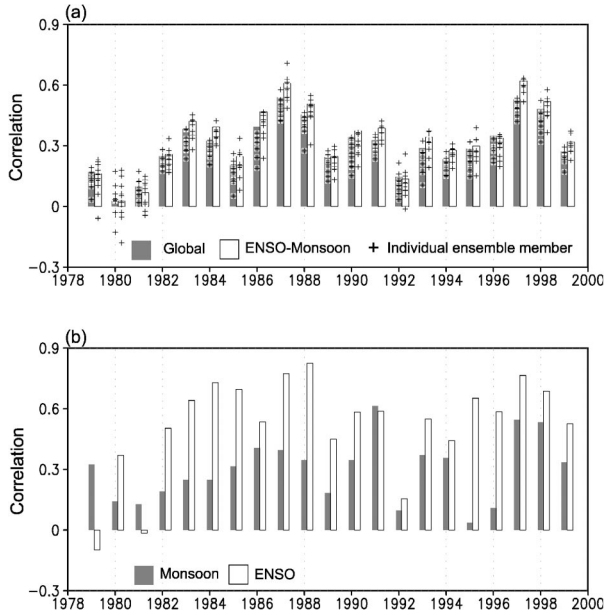

FIG. 6. Pattern correlation coefficients between the observed and predicted ensemble-mean precipitations (a) over the globe (shaded bar) and the ENSO–monsoon region (30°S–30°N and 40°E–80°W; open bar) and (b) over the monsoon region (30°S–30°N and 40°–160°E; shaded bar) and the ENSO region (30°S–30°N and 160°E–80°W; open bar). In (a), the pattern correlation coefficients of the individual ensemble member are marked by crosses.

similarly to that of the globe, indicating that the global precipitation variability is mainly controlled by the precipitation variation over the ENSO–monsoon region, where relatively large precipitation prevails in the summer. It is also noted that the correlation value is relatively large for both the warm and cold phases of ENSO with the exception of 1982.

The spatial correlations are also obtained for the monsoon (30°S–30°N, 40°–160°E) and ENSO (30°S–30°N, 160°E–80°W) regions, separately, and their year to year variations are shown in Fig. 6b. The correlation values for the ENSO region are large (bigger than 0.6) for most of the El Niño events and relatively large even in normal years, for example, 1980, 1986, 1990, 1995, and so on. However, the monsoon precipitation is not well predicted in most of the summers. It is also noted that the prediction skill in the monsoon region is typically not related to the ENSO. The poor predictability is mainly due to poor performance of the model in the western Pacific. This poor performance in the western Pacific is related to the model systematic error as shown in the previous section, which will be discussed in more detail in the next section.

5. Prediction skill after correction

a. Error correction and verification methods

A correction procedure of the model bias can be developed based on the statistical relationship between the model and observation. The most commonly used methods developed to date are based on singular value decomposition (SVD) analysis and canonical correlation analysis (CCA) of the observation and model output (Barnstorn and Smith 1996; Ward and Navarra 1997; Feddersen et al. 1999). In the present study, the error correction method is developed in terms of leading SVD modes as described in Feddersen et al. (1999). Before obtaining a transfer function between two anomaly fields, EOF analysis is applied to the simulated and observed anomalies, separately, to reduce the spatial dimensions. Here the observed and predicted fields are reconstructed by retaining the leading 10 EOF modes of each field. After that, the SVD analysis is used to extract coupled modes between the two anomaly fields. The systematic errors of the simulated anomaly are corrected by replacing the simulated modes to the corresponding observed modes. The transfer function for the replacement can be constructed as follows:

$$X(x, t) = \sum_{i=1}^{P} \alpha_i Y_i(t) R_i(x), \tag{3}$$

where $X(x, t)$ is the corrected field, $Y(t)$ is the time coefficients of the SVD mode for the simulated field, and $R(x)$ is the projection of SVD singular vector onto the observed field; i is the mode number, P the total number of the SVD modes, and α is the correlation coefficient between the time series of the SVD mode of prediction and the corresponding SVD time series of the observation.

Double cross validation (Kaas et al. 1996) is used to evaluate the skill of the bias-corrected prediction anomalies. The relatively short period of record, 21 yr, utilized in the present study may produce overestimated skill scores by overfitting random variability as indicated by Davis (1976). To control this kind of problem, SVD analysis is repeatedly applied to data from which 1 yr is excluded and the error correction is made for that year. In addition, in each step of the cross-validation procedure, cross-validated expansion coefficients of the SVD modes are computed in order to select which modes to include in the bias correction. That is, the predictive skill of the individual modes is assessed a priori by determining the correlations between the cross-validated expansion coefficients. Details of the present verification procedure can be found in Feddersen et al. (1999).

It is noted that the adjustment of the prediction toward the observation based on the SVD leads to a loss of variability in absolute magnitude; that is, the adjusted field stays close to the climatology. Thus, it may be necessary to apply some sort of inflation method to the adjusted field. The most common method for this type of inflation is to multiply the adjusted values by the ratio between the standard deviation of the observations and that of the adjusted values. In the present study, the inflation factor is obtained by combining the common method of inflation and the weighting factor considered by Feddersen et al. (1999). The weighting factor depends on the magnitude of the local variability of the adjusted field. This approach leaves grid points of small variability, which usually have little skill, uninflated, while concentrating the inflation on more skillful grid points with large variability. The inflation factor IF_k in a grid point k is defined here as

$$\mathrm{IF}_k = \frac{\sigma_{k,\mathrm{obs}}}{\sigma_{k,\mathrm{fct}}} w\left(\frac{\sigma_{k,\mathrm{fct}}}{\sigma_{\mathrm{max,fct}}}\right), \tag{4}$$

where $\sigma_{k,\mathrm{obs}}$ is the standard deviation of the observation, $\sigma_{k,\mathrm{fct}}$ is that of the bias-corrected simulation anomaly, $\sigma_{\mathrm{max,fct}}$ is the maximum value of $\sigma_{k,\mathrm{fct}}$, and $w(x)$ is an s-shaped weight function $w(x) = \{1 + \tanh[6.9(x - 0.5)]\}/2$, which is close to zero for $x = 0$ and close to one for $x = 1$.

b. Predictability after error correction

The impact of the bias correction on the prediction of the global precipitation is examined in this section. Before making the correction, we examined how well the model reproduces the EOF eigenmodes of the precipitation variability over the globe. Figure 7a shows the first eigenvector of the observed summer-mean precipitation, which explains 24.3% of total variance, and Fig. 7c is the predicted counterpart, explaining 39.0%

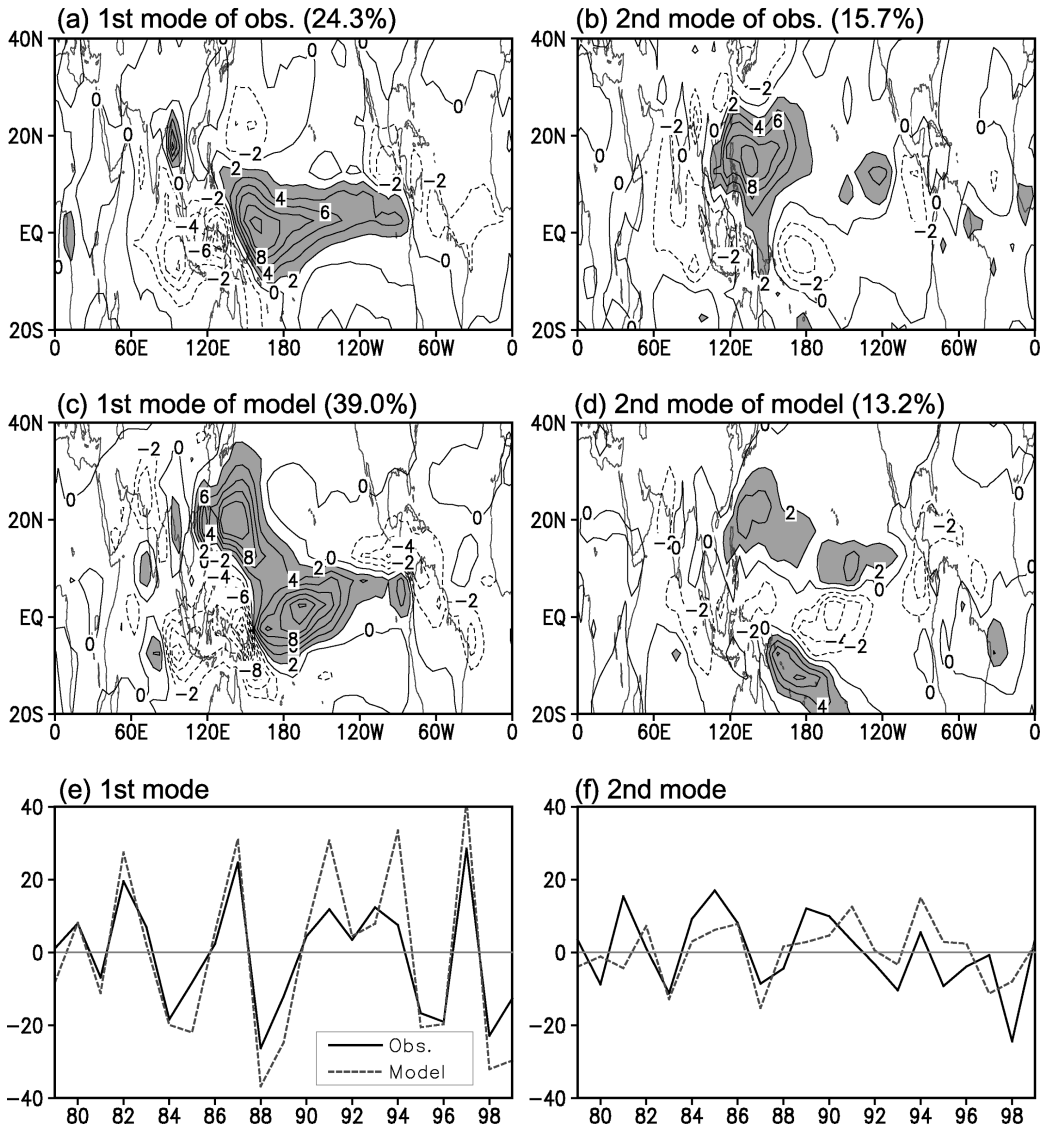

FIG. 7. EOF modes of the observed and simulated ensemble-mean precipitation. (a), (b) The observed first and second eigenvectors; (c), (d) the simulated counterparts, and (e), (f) the time series associated with the eigenvectors. Solid and dashed lines indicate the observed and simulated time series, respectively.

of the total variance. Both figures are characterized by an east–west seesaw pattern between the anomalies in the tropical central Pacific and the Indonesian subcontinent, although the model centers are shifted to the east. Other noticeable differences include sign differences in the subtropical western Pacific and the Indian Ocean eastward from 60°E. The poor performance of the model in those regions has already been mentioned in the previous section. The time series associated with the eigenvectors, shown in Fig. 7e, vary in a similar way and are related to ENSO SST anomalies. The difference between the model and observed eigenvectors in the subtropical western Pacific and Indian Oceans is due to the failure of the model simulation in response to ENSO SST anomalies. The poor simulation over the regions can be related to the limitation of the two-tier approach of the seasonal prediction, since the atmospheric responses to those ocean regions are controlled not simply by the atmosphere alone but by the ocean–atmosphere interaction (Wang et al. 2004).

The second eigenvector of the observed summer-mean precipitation shown in Fig. 7b explains 15.7% of total variance. The spatial pattern is characterized by large variations in the subtropical western Pacific. The model counterpart, shown in Fig. 7d, shows that the model reproduces the western Pacific center but with much weaker amplitude. It also produces anomalies in other regions in the Pacific and Indian Oceans that are somewhat different from the observations. However, the similarity between the time series associated with the

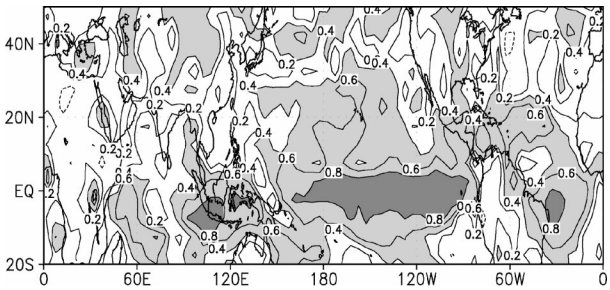

FIG. 8. As in Fig. 5 except for the predicted precipitation after correction of the systematic error.

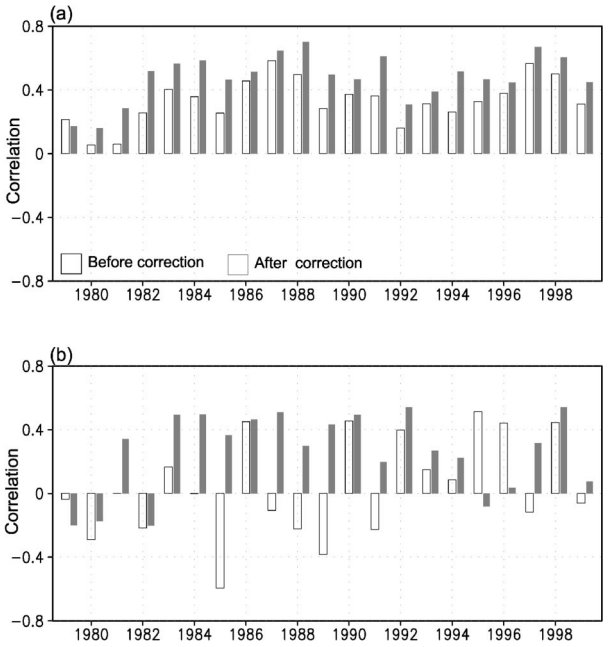

FIG. 9. Pattern correlation coefficients between the observed and predicted precipitation before (open bar) and after (shaded bar) the bias correction (a) over the globe and (b) for the Asian monsoon and western Pacific regions (10°–40°N, 80°–160°E).

observed EOF modes and the corresponding time series of the predicted modes provides us some hope of error correction for the predicted field. That is, the atmosphere model captures the observed eigenmodes responding to distinctive SST anomaly patterns such as El Niño, although the spatial patterns of the modes are somewhat different from their observed counterparts. The difference can be corrected by replacing the model eigenmodes with the corresponding observed modes. The error correction has been done by using Eq. (2) and the SVD modes, which represent more clearly the coupled modes of the observed and predicted fields than the EOF modes do. Note that the two leading SVD singular vectors (not shown) are very similar to the corresponding EOF eigenvectors shown in Fig. 7. The similarity can be anticipated from Figs. 7e and 7f, where the two time series of the observed and predicted vary almost simultaneously, indicating that the two EOF modes are coupled to each other.

In each summer and at each grid point, the number of SVD modes is determined by the double cross-validation procedure. In general, the first four SVD modes are used for the correction. The modes after the fifth consist of small-scale patterns and explain small fractions of the variance. The sum of the first four modes explains 41.2% of the total variance.

Figure 8 shows the spatial distribution of the correlation coefficient between the corrected seasonal prediction and the corresponding observation, obtained from the double cross-validation procedure described in the previous section. The figure shows the potential predictability of the seasonal prediction after correction, when the actual SST is used for the prediction. In the figure, the correlation coefficients of the corrected prediction are replaced by those without correction, if the former is smaller than the latter. Those locations are in the central tropical Pacific, where the correlation coefficient of the original prediction (Fig. 3) is already very large. But, in most of the regions, the predictability is significantly enhanced by the statistical correction. The enhancement of the predictability is particularly pronounced in the western Pacific where the correction skill is negative without the correction but has relatively large positive values afterward.

The predictability skill is also examined in terms of the spatial pattern correlation between the observed and predicted fields of each year for the domain of 20°S–50°N and 0°–360° (Fig. 9a). In Fig. 9a, the open and shaded bars indicate the pattern correlations for the predictions without and with correction, respectively. As seen in the figure, the potential predictability is enhanced by the correction for all years except the first (1979) summer. The same correlations are also obtained for the Asia monsoon and the western Pacific region, where the original prediction is poor, and are plotted in Fig. 9b. It is clear that the correction enhances the predictability skill over the domain in most of the years. In particular, for the years such as 1985, 1987–89, and 1991, the spatial correlations with negative values before the correction have relatively large positive values after the correction. In the years 1995 and 1996, on the other hand, the skill is degraded by the correction. Overall, however, the dynamical prediction with the statistical correction appears to have potential skill over East Asia and the western Pacific region.

It would be interesting to know the regions where the statistical correction has its largest impact on the prediction skill. To help determine this, we divided the error, E = Prediction (P) − Observation (O), into a corrected part ($P - C$) and a noncorrectable error part ($C - O$), where C stands for the corrected value. The variance of E was shown in Fig. 4a. Figures 10a and 10b show the variances of the corrected and noncorrectable parts, respectively. Note that the sum of the two variances is approximately the same as the variance of

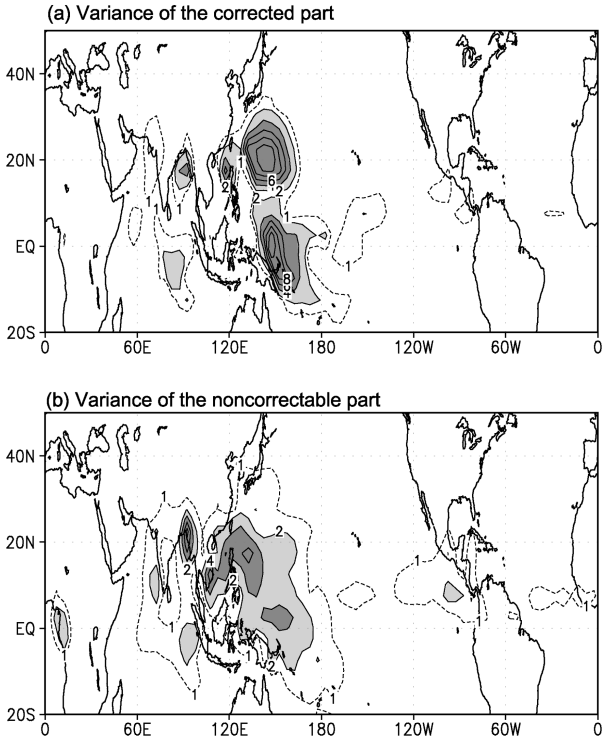

FIG. 10. Variances of the (a) corrected part and (b) noncorrectable part of the systematic error. See text for the definitions of corrected and noncorrected parts. The contour interval is 2 mm^2 day^{-2} and the dashed line indicates 1 mm^2 day^{-2}.

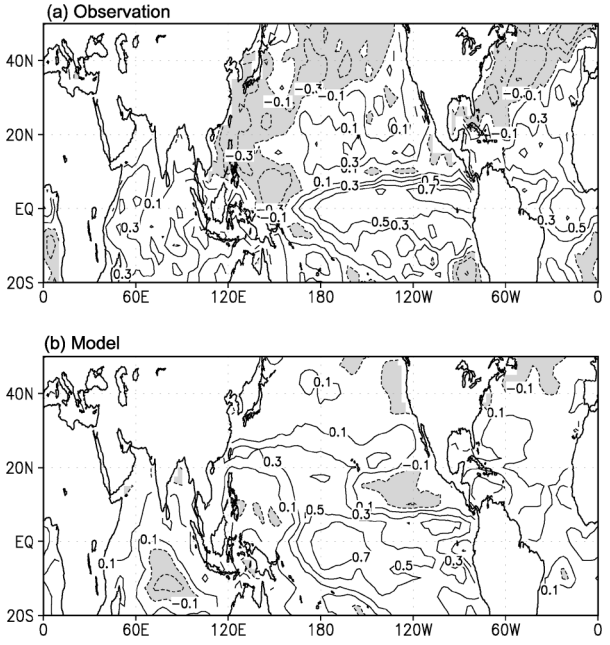

FIG. 11. (a) Distribution of the local correlation coefficient between the observed precipitation and the SST anomalies at each grid point. (b) As in (a) except for the simulated precipitation. The contour interval is 0.2.

the total error shown in Fig. 4a. Figure 10a indicates that the SVD-based postprocessing method reduces the prediction errors, particularly over the western Pacific in the Northern and Southern Hemispheres. Those errors are mainly related to poor simulation of the precipitation anomalies in the western Pacific during El Niño, as indicated by the difference between the first EOF modes of the observed and the predicted anomalies, shown in Figs. 7a and 7c, respectively. As a result, the variance of the noncorrectable error is much reduced (Fig. 10b).

The errors in the western Pacific are correctable because they are systematic. These systematic errors can be produced by the model deficiency itself but appear to be related largely to the prescription of the SST condition in the prediction system. In the western Pacific where the air–sea interaction is active, the SST is also strongly affected by the atmosphere (Wang and Xie 1998; Lau and Nath 1999). But in the present two-tier prediction system, the model atmosphere is a slave to the prescribed SST condition and the atmospheric feedback to the ocean is missing. In the model, in fact, the predicted precipitation anomalies are positively related to the local SST anomalies in most of the western Pacific (Fig. 11b). In the observations, on the other hand, the local SST and precipitation anomalies are negatively correlated to each other in the subtropical western Pacific (Fig. 11a). This difference between the SST–precipitation relationships of the observation and the model results in the systematic errors in the western Pacific. But, they are largely correctable by using the present postprocessing method.

6. Summary and concluding remarks

The potential predictability of summer-mean precipitation over the globe is investigated in the present study. The data utilized in the present study are obtained from a 21-yr seasonal prediction experiment using the KMA–SNU seasonal prediction system under the guidance of Seasonal Model Intercomparison Project II (SMIP II) initiated by the CLIVAR/Working Group on Seasonal to Interannual Prediction (WGSIP). The potential predictability assessed in the present study is an upper-limit estimate of the predictability of the prediction system, since the SMIP II uses the observed SST as an external boundary condition for the model integration of seasonal prediction.

Potential predictability measured by the analysis of variance indicates that the external SST condition controls the summer-mean precipitation in the Tropics, particularly in the ENSO region. On the other hand, the extratropical summer mean is more controlled by the internal atmospheric processes. The result indicates that the summer-mean precipitation over the Asian monsoon and ENSO regions is potentially predictable, if the model is perfect. Over the ENSO region, the present model has the capability to reproduce the observed interannual variation of the precipitation for a given SST condition.

Over the Asian monsoon region, on the other hand, the model is not able to reproduce the summer-mean precipitation even given the actual SST condition. This failure can be due to the problem of the present atmosphere model itself. However, it is also possible that the Asian monsoon precipitation, particularly in the western Pacific, is not simply related to the SST anomalies but is mainly controlled by the feedback processes of atmosphere–ocean interaction. The importance of the air–sea interaction on the circulation anomalies in the western Pacific associated with the evolution of ENSO has been demonstrated by Wang and Xie (1998) with observed data and Lau and Nath (1999) using models. As shown in Fig. 11, the difference between the SST–precipitation relationships of the observation and the model results in the systematic errors in the western Pacific. Therefore, the present two-tier approach of seasonal prediction, based on the atmospheric model simulation with a prescribed future SST condition, may not be adequate for the seasonal prediction of Asian summer monsoon.

The present model is capable of predictability of the summer-mean precipitation in only some of the tropical region, particularly in the tropical central and eastern Pacific. Although the simulation is poor, the predictability of the Asian summer monsoon can be improved since the model errors are systematic and related to the external SST condition. In the present study, these errors are shown to be correctable by a statistical relationship between the observation and the model prediction. In particular, the improvement of the predictability after the statistical correction is substantial in the subtropical western Pacific. The error in the subtropical Pacific is discernable in the first EOF eigenvector and the SVD singular vector of model summer-mean precipitation, and this mode is related to the poor simulation of the observed ENSO mode in the region. After the correction, the correlation skill of the summer-mean precipitation is usable in most of the western Pacific. It is also shown that the statistical correction is more effective for the East Asian and western Pacific regions if the correction procedure based on the SVD is applied to the regional data rather than the global data. Now the question is how to predetermine the region of analysis. At the moment, the region of best predictability may be chosen by trial and error using different regional domains.

The correction method in the present study has been developed based on the global SVD modes. But, some of the regional precipitation variability can be controlled by regional modes, which may not be represented in the global modes, since the precipitation has a strong local gradient particularly in the Asian monsoon region. Thus the correction method for the regional precipitation can be developed based on the SVD modes over the domain. The statistical correction can also be developed for each grid point based on the relationship between the observed variability at the grid point and the model-simulated pattern. Then the prediction value at the grid point can be produced by projecting the model pattern known a priori to the predicted field. Various kinds of correction methods mentioned above should be developed and tested for a better seasonal prediction. Other research to be done includes the examination of the potential predictability of other seasons and the application of the present correction method to other variables such as surface temperature and circulation statistics. The present study has examined the potential predictability by prescribing the observed SST condition in the model, and therefore we assessed the upper limit of the predictability of the present seasonal prediction system. It has been demonstrated here that the present seasonal prediction system has large potential predictability in many regions of the globe, particularly in Asian monsoon and ENSO regions. But the actual predictability should depend on the skill in predicting SST. Therefore, research into a better SST prediction system is required to produce a usable seasonal prediction. It is also worth noting that the development of a seasonal prediction system based on a coupled ocean–atmosphere model may be needed, particularly for the Asia and western Pacific monsoon regions, since the western Pacific summer-mean precipitation appears to be largely controlled by air–sea feedback processes.

Acknowledgments. The present study is supported by the Korean Meteorological Administration and Korea Computer Science Institute. This study was carried out in the Climate Environment System Research Center (CES), which is sponsored by the Korea Science and Engineering Foundation.

REFERENCES

Barnett, T. P., and R. Preisendorfer, 1987: Origins and levels of monthly and seasonal forecast skill for United States surface air temperatures determined by canonical correlation analysis. *Mon. Wea. Rev.,* **115,** 1825–1850.

Barnston, A. G., 1994: Linear statistical short-term climate predictive skill in the Northern Hemisphere. *J. Climate,* **7,** 1513–1564.

——, and T. M. Smith, 1996: Specification and prediction of global surface temperature and precipitation from global SST using CCA. *J. Climate,* **9,** 2660–2697.

Bonan, G. B., 1998: The land surface climatology of the NCAR land surface model coupled to the NCAR Community Climate Model. *J. Climate,* **11,** 1307–1326.

Davis, R. E., 1976: Predictability of sea surface temperature and sea level pressure anomalies over the North Pacific Ocean. *J. Phys. Oceanogr.,* **6,** 249–266.

Dix, M. R., and B. G. Hunt, 1995: Chaotic influences and the problem of deterministic seasonal predictions. *Int. J. Climatol.,* **15,** 159–164.

Feddersen, H., A. Navarra, and M. N. Ward, 1999: Reduction of model systematic error by statistical correction for dynamical seasonal prediction. *J. Climate,* **12,** 1974–1989.

Goswami, B. N., 1998: Interannual variations of Indian summer monsoon in a GCM: External conditions versus internal feedbacks. *J. Climate,* **11,** 501–522.

Graham, N. E., P. Barnett, R. Wilde, M. Ponater, and S. Schubert, 1994: On the roles of tropical and midlatitude SSTs in forcing

interannual to interdecadal variability in the winter Northern Hemisphere circulation. *J. Climate,* **7,** 1416–1441.

Holtslag, A. A. M., and B. A. Boville, 1993: Local versus nonlocal boundary layer diffusion in a global climate model. *J. Climate,* **6,** 1825–1842.

Kaas, E., T.-S. Li, and T. Schmith, 1996: Statistical hindcast of wind climatology in the North Atlantic and northwestern European region. *Climate Res.,* **7,** 97–110.

Kang, I.-S., and Coauthors, 2002a: Intercomparison of GCM simulated anomalies associated with the 1997–98 El Niño. *J. Climate,* **15,** 2791–2805.

——, and Coauthors, 2002b: Intercomparison of the climatological variations of Asian summer monsoon precipitation simulated by 10 GCMs. *Climate Dyn.,* **19,** 383–395.

Kim, J.-K., I.-S. Kang, and C.-H. Ho, 1998: East Asian summer monsoon simulated by the Seoul National University GCM. *Proc. Int. Conf. on Monsoon and Hydrologic Cycle,* Kyongju, South Korea, Korean Meteorological Society, 66–69.

Kumar, A., and M. P. Hoerling, 1995: Prospects and limitations of seasonal atmospheric GCM predictions. *Bull. Amer. Meteor. Soc.,* **76,** 335–345.

Kusunoki, S., M. Sugi, A. Kitoh, C. Kobayashi, and K. Takano, 2001: Atmospheric seasonal predictability experiments by the JMA AGCM. *J. Meteor. Soc. Japan,* **79,** 1183–1206.

Lau, N.-C., and M. J. Nath, 1999: Observed and GCM-simulated westward-propagating, planetary-scale fluctuations with approximately three-week periods. *Mon. Wea. Rev.,* **127,** 2324–2345.

Lorenz, E. N., 1960: Maximum simplification of the dynamic equations. *Tellus,* **12,** 243–254.

McFarlane, N. A., 1987: The effect of orographically excited gravity wave drag on the general circulation of the lower stratosphere and troposphere. *J. Atmos. Sci.,* **44,** 1775–1800.

Moorthi, S., and M. J. Suarez, 1992: Relaxed Arakawa–Schubert: A parameterization of moist convection for general circulation models. *Mon. Wea. Rev.,* **120,** 978–1002.

Nakajima, T., and M. Tanaka, 1986: Matrix formulation for the transfer of solar radiation in a plane-parallel scattering atmosphere. *J. Quant. Spectrosc. Radiat. Transfer,* **35,** 13–21.

Normand, C., 1953: Monsoon seasonal forecasting. *Quart. J. Roy. Meteor. Soc.,* **79,** 463–473.

Ramage, C. S., 1971: *Monsoon Meteorology.* Academic Press, 296 pp.

Rowell, D. P., 1996: Reply to comments by Y. C. Sud and W. K.-M. Lau on Variability of summer rainfall over tropical North Africa (1906–92): Observations and modeling by D. P. Rowell, C. K. Folland, K. Maskell, and M. N. Ward (April 4, 1995, 121, 669–704): Further analysis of simulated interdecadal North Africa. *Quart. J. Roy. Meteor. Soc.,* **122,** 1007–1013.

——, 1998: Assessing potential seasonal predictability with an ensemble of multidecadal GCM simulations. *J. Climate,* **11,** 109–120.

——, C. K. Folland, K. Maskell, and M. N. Ward, 1995: Variability of summer rainfall over tropical North Africa (1906–92): Observations and modeling. *Quart. J. Roy. Meteor. Soc.,* **121,** 669–704.

Sperber, K. R., and T. N. Palmer, 1996: Interannual tropical rainfall variability in general circulation model simulations associated with the Atmosphere Model Intercomparison Project. *J. Climate,* **9,** 2727–2750.

——, and Coauthors, 2001: Dynamical seasonal predictability of the Asian summer monsoon. *Mon. Wea. Rev.,* **129,** 2226–2247.

Stern, W., and K. Miyakoda, 1995: The feasibility of seasonal forecasts speculated from multiple GCM simulations. *J. Climate,* **8,** 1071–1085.

Terjung, W. H., L. O. Mearns, P. E. Todhunter, J. T. Hayes, and H.-Y. Ji, 1989: Effects of monsoon fluctuations on grains in China. Part II: Crop water requirements. *J. Climate,* **2,** 19–38.

Wang, B., and X. Xie, 1998: Coupled modes of the warm pool climate system. Part I: The role of air–sea interaction in maintaining Madden–Julian oscillation. *J. Climate,* **11,** 2116–2135.

——, and LinHo, 2002: Rainy season of the Asian–Pacific summer monsoon. *J. Climate,* **15,** 386–398.

——, I.-S. Kang, and J.-Y. Lee, 2004: Ensemble simulation of Asian–Australian monsoon variability by 11 AGCMs. *J. Climate,* **17,** 803–818.

Ward, M. N., and A. Navarra, 1997: Pattern analysis of SST-forced variability in ensemble GCM simulations: Examples over Europe and the tropical Pacific. *J. Climate,* **10,** 2210–2220.

Xie, P., and P. A. Arkin, 1997: Global precipitation: A 17-year monthly analysis based on gauge observation, satellite estimates, and numerical model outputs. *Bull. Amer. Meteor. Soc.,* **78,** 2539–2558.

Zwiers, F. W., 1996: Interannual variability and predictability in an ensemble of AMIP climate simulations conducted with the CCC GCM2. *Climate Dyn.,* **12,** 825–847.